Polymer 50 (2009) 685–695

Contents lists available at ScienceDirect

Polymer

journal homepage: www.elsevier.com/locate/polymer

Self-assembly behavior of hepta(3,3,3-trifluoropropyl) polyhedral oligomeric silsesquioxane-capped poly(ε-caprolactone) in epoxy resin: Nanostructures and surface properties

Ke Zeng [a], Lei Wang [a], Sixun Zheng [a,*], Xuefeng Qian [b]

[a] Department of Polymer Science and Engineering and State Key Laboratory of Metal Matrix Composites, Shanghai Jiao Tong University, 800 Dongchuan Road, Shanghai 200240, PR China
[b] Department of Chemistry, Shanghai Jiao Tong University, Shanghai Jiao Tong University, Shanghai 200240, PR China

ARTICLE INFO

Article history:
Received 11 July 2008
Received in revised form
14 November 2008
Accepted 15 November 2008
Available online 25 November 2008

Keywords:
Polyhedral oligomeric silsesquioxane
Epoxy
Self-assembly

ABSTRACT

The organic–inorganic amphiphile, hepta(3,3,3-trifluoropropyl) polyhedral oligomeric silsesquioxane (POSS)-capped poly(ε-caprolactone) (POSS-capped PCL) was synthesized *via* the ring-opening reaction of ε-caprolactone, which was initiated by 3-hydroxypropylhepta(3,3,3-trifluoropropyl) polyhedral oligomeric silsesquioxane (POSS) with stannous (II) octanoate [$Sn(Oct)_2$] as the catalyst. The organic–inorganic nanocomposites were prepared *via* the *in situ* polymerization of epoxy monomers in the presence of the POSS-capped PCL. The atomic force microscopy (AFM) shows that the organic–inorganic hybrids possess the nanostructures. In view of the miscibility of the sub-components of the organic–inorganic amphiphile [*i.e.*, PCL chains and POSS cages] with epoxy after and before curing reaction, the formation of the nanostructures in the thermosets followed the mechanism of self-assembly. The surface properties of the organic–inorganic nanocomposites were investigated by means of static contact angle measurements and X-ray photoelectronic spectroscopy (XPS). It is demonstrated that the improvement in surface hydrophobicity was ascribed to the enrichment of the POSS cages on the surface of the materials.

1. Introduction

The concept of incorporating inorganic blocks into organic polymers has been widely accepted to obtain the materials with improved properties *via* the formation of organic–inorganic hybrids during the past decades [1–6]. Organic–inorganic composites can combine the advantages of both inorganic and organic materials. The properties of the hybrid composites are greatly dependent on the dispersion of inorganic components in the organic matrix. It is recognized that the nanoscaled dispersion of inorganic components in polymeric matrix can greatly optimize the inter-component interactions and the properties of materials are thus improved. However, the big difference in solubility parameter between inorganic components and organic polymers would give rise to the macroscopic phase separation in organic–inorganic composite systems unless the specific measurements were taken to suppress the tendency of the macroscopic demixing. In practice, organic–inorganic nanocomposites can be prepared *via* sol–gel process [2,3], intercalation and exfoliation of layered silicates by organic polymers [4–6]. In sol–gel process, the fine dispersion of inorganic nanoparticles is fulfilled *via* hydrolysis and condensation of silanes bearing organic ligands so that the affinity can be formed between organic polymers and inorganic components. For preparation of layered silicates containing nanocomposites, the pristine layered silicates must be organically modified to achieve intercalation or exfoliation of layers of silicates.

Polyhedral oligomeric silsesquioxane (POSS) reagents, monomers, and polymers are emerging as a new chemical technology for preparing the organic–inorganic hybrid nanocomposites. A typical POSS molecule possesses the structure of cube-octameric frameworks represented by the formula ($R_8Si_8O_{12}$) with an inorganic silica-like core (Si_8O_{12}) (~0.53 nm in diameter) surrounded by eight organic corner groups, one or more of which is reactive (Scheme 1). The reactive POSS has been incorporated into organic polymers *via* copolymerization or reactive grafting approaches. Relatively, the nanocomposites prepared *via* direct physical blending of POSS with organic polymers was less reported possibly due to the unfavorable miscibility (or solubility) of silsesquioxanes with organic polymers. During the past years, considerable attention has been paid to incorporate POSS into thermosets to access organic–inorganic nanocomposites [7–19]. Lee and Lichtenhan [7] reported that the molecular level reinforcement provided by a monofunctional POSS could significantly retard the physical aging process of epoxy thermosets in the glassy state. Laine et al. [8–13] investigated the

* Corresponding author. Tel.: +86 21 54743278; fax: +86 21 54741297.
E-mail address: szheng@sjtu.edu.cn (S. Zheng).

0032-3861/$ – see front matter © 2008 Elsevier Ltd. All rights reserved.
doi:10.1016/j.polymer.2008.11.024

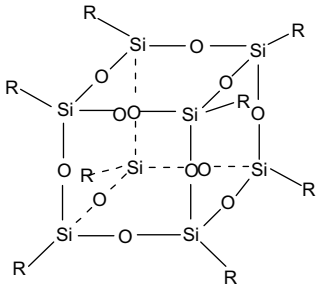

Scheme 1. Structure of POSS.

modifications of epoxy by a series of octasilsesquioxanes with a variety of reactive R groups such as aminophenyl, dimethylsiloxypropylglycidyl ether groups and found that the dynamic mechanical properties, fracture toughness and thermal stability of the epoxy hybrids were closely dependent on the types of R groups, tether structures between epoxy matrices and POSS cages and the defects in silsesquioxane cages, etc. Williams et al. [14] observed that a primary liquid–liquid phase separation occurred at the time of adding the POSS-diamine precursors to epoxy due to the incompatibility between epoxy and heptaisobutyl glycidyl POSS. It is noted that the nature of the organic inert groups and pre-reaction of a monofunctional POSS have pronounced impact on the morphology of the resulting POSS-modified polymer networks [15]. Zheng et al. [16] reported that the different morphological structures could be formed in the POSS-containing hybrid composites depending on the types of R groups; moreover, the phase-separated composites and nanocomposites could be prepared by adjusting the degrees of reaction between epoxy matrix and POSS macromer. Matejka et al. [17,18] investigated the structure and properties of epoxy networks reinforced with POSS and it was identified that the POSS–POSS interactions have a profound impact on the thermomechanical properties of the materials.

Most of the previous studies reported the incorporation of POSS into thermosetting polymers *via* the chemical approaches, *i.e.*, the chemical bonds between POSS and polymer matrix are formed to suppress the tendency of macroscopic phase separation of POSS, however, only a few reports were involved with the preparation of POSS-containing hybrid thermosets *via* physical blending [16,20–25]. In the present work, we designed and synthesized hepta(3,3,3-trifluoropropyl) POSS-capped poly(ε-caprolactone) (PCL), a novel organic–inorganic amphiphile. It has a tadpole-like topology, which is composed of an organic "tail" (*viz.* PCL chain) and inorganic "head" (*viz.* POSS cage) portions. The organic–inorganic amphiphile was incorporated into epoxy resin to access the organic–inorganic hybrid nanocomposites based on the following knowledge: (i) PCL subchain is miscible with epoxy after and before the curing reaction and (ii) the POSS is immiscible with epoxy resin after and before curing reaction. Therefore, it is expected that the nanostructures in epoxy thermosets can be accessed *via* a self-assembly approach. In addition, the POSS block of the POSS-capped PCL contains organosilicon and organofluorine moieties and thus is of low free energy [25–32] and the enrichment of the POSS portion at the surface of the nanocomposites could occur upon incorporating the organic–inorganic amphiphile into organic polymers and thus the surface hydrophobicity of the hybrid thermosets could be significantly enhanced. In this work, atomic force microscopy (AFM), differential scanning calorimetry (DSC) and thermogravimetric analysis (TGA) were used to investigate the morphology and the thermal properties of the thermosets. The surface properties of the nanostructured thermosets were addressed on the basis of static contact angle measurements and X-ray photoelectronic spectroscopy (XPS).

2. Experimental

2.1. Materials

3,3,3-Trifluoropropyltrimethoxysilane was purchased from Zhejiang Chem-Technology Co., China. 3-Chloropropyl trichlorosilane was obtained from Shanghai Lingguang Chemical Co., China and was used as-received. The monomer, ε-caprolactone (CL), was purchased from Fluka Co., Germany; it was distilled over CaH_2 under decreased pressure before use. Unless specially indicated, other reagents such as sodium, calcium hydride (CaH_2), $AgNO_3$, stannous (II) octanoate [$Sn(Oct)_2$] and sodium hydroxide (NaOH) were of chemically pure grade, purchased from Shanghai Reagent Co., China. The solvents such as tetrahydrofuran (THF), dichloromethane, petroleum ether (distillation range: 60–90 °C) and triethylamine (TEA) were of chemically pure grade, also obtained from commercial resources. Before use, THF was refluxed above sodium and then distilled and stored in the presence of the molecular sieve of 4 Å. Triethylamine (TEA) was refluxed over CaH_2 and then was purified with *p*-toluenesulfonyl chloride, followed by distillation.

2.1.1. Synthesis of 3-chloropropylhepta(3,3,3-trifluoropropyl) POSS

In the first step, hepta(3,3,3-trifluoropropyl)tricycloheptasiloxane trisodium silanolate [$Na_3O_{12}Si_7(C_3H_4F_3)_7$] was synthesized by following the method reported by Fukuda et al. [25]. In a typical experiment, (3,3,3-trifluoropropyl) trimethoxysilane (50.0 g, 0.23 mol), THF (250 ml), deionized water (5.25 g, 0.29 mol) and sodium hydroxide (3.95 g, 0.1 mol) were charged to a flask equipped with a condenser and a magnetic stirrer. After refluxed for 5 h, the reactive system was cooled down to room temperature and held at this temperature for 15 h with vigorous stirring. All the solvents and other volatiles were removed by rotary evaporation and the white solids were obtained. After drying at 40 °C *in vacuo* for 12 h, 37.3 g products were obtained with the yield of 98%. 3-Chloropropylhepta(3,3,3-trifluoropropyl) polyhedral oligomeric silsesquioxane was prepared *via* the corner-capping reaction between $Na_3O_{12}Si_7(C_3H_4F_3)_7$ and 3-chloropropyl trichlorosilane. Typically, $Na_3O_{12}Si_7(C_3H_4F_3)_7$ (10.0 g, 8.8 mmol) and triethylamine (1.3 ml, 8.8 mmol) were charged to a flask equipped with a magnetic stirrer, 200 ml anhydrous THF were added with vigorous stirring. The flask was immersed into an ice-water bath and purged with highly pure nitrogen for 1 h. After that, 3-chloropropyl trichlorosilane (2.24 g, 0.56 mmol) dissolved in 20 ml anhydrous THF was slowly dropped within 30 min. The reaction was carried out at 0 °C for 4 h and at room temperature for 20 h. The sodium chloride was filtered out and the solvent together with other volatiles was removed *via* rotary evaporation to afford the white solids. The solids were washed 3 times with 50 ml methanol and dried *in vacuo* at 40 °C for 24 h and the product of 7.53 g was obtained with the yield of 73%. FTIR (cm^{-1}, KBr window): 1090–1000 (Si–O–Si), 2900–2850 ($-CH_2$), 1120–1300 ($-CF_3$). ^{1}H NMR (ppm, acetone-d_6): 3.62 (*t*, 2.0**H**, –C**H$_2$**–Cl), 2.32 (*m*, 14.0**H**, $SiCH_2C\mathbf{H_2}CF_3$), 1.93 (*m*, 2.0**H**, –C**H$_2$**–CH_2–Cl), 1.03 (*m*, 14.0**H**, $SiC\mathbf{H_2}CH_2CF_3$), 0.93 (*t*, 2.0**H**, –C**H$_2$**–CH_2–CH_2–Cl). ^{13}C {H} NMR (ppm, acetone-d_6): 4.28 (*m*, Si–**C**H_2–CH_2–CF_3), 27.4 (*m*, –CH_2–**C**H_2–CF_3, $J = 23$ Hz), 128.5 (*tetra*, –CH_2–CH_2–**C**F_3, $J = 274$ Hz); 9.38 (*m*, Si–**C**H_2–CH_2–CH_2Cl), 26.5 (*s*, –CH_2–**C**H_2–CH_2Cl), 47.6 (*s*, –CH_2–CH_2–**C**H_2Cl); ^{29}Si NMR (ppm, acetone-d_6): −70.1 (*s*, 1.1**Si**), −69.2 (*s*, 3.0Si), −66.7 (*s*, 3.1Si) and −65.9 (*s*, 1.0Si).

2.1.2. Synthesis of 3-hydroxypropylhepta(3,3,3-trifluoropropyl) POSS

3-Hydroxypropylhepta(3,3,3-trifluoropropyl) POSS was prepared *via* the hydrolysis of 3-chloropropylhepta(3,3,3-trifluoropropyl) POSS in the presence of fresh silver oxide (Ag_2O). Typically, 3-chloropropylhepta(3,3,3-trifluoropropyl) POSS (10.0 g, 9.38 mmol)

was charged to a 500 ml flask equipped with a magnetic stir bar. The mixture of 200 ml THF with 200 ml ethanol, deionized water (5 ml) and fresh Ag_2O (3.0 g) was added. The system was refluxed for 24 h and all the insoluble solids were filtered out. The above procedure was repeated for 3 times to ensure the complete conversation of 3-chloropropylhepta(3,3,3-trifluoropropyl) POSS into 3-hydroxypropylhepta (3,3,3-trifluoropropyl) POSS. After that, all the solvents were removed by rotary evaporation. After dried *in vacuo* at 60 °C for 24 h, 8.36 g solid products were obtained with the yield of 85%. FTIR (cm^{-1}, KBr window): 3336 (O–H), 1090–1000 (Si–O–Si), 2900–2850 (–CH_2), 1120–1300 (–CF_3). ^{1}H NMR (ppm, acetone-d_6): 3.61 (*t*, 2.0**H**, –C**H$_2$**–OH), 2.32 (*m*, 14.0**H**, SiCH$_2$C**H$_2$**CF$_3$), 1.93 (*m*, 2.0**H**, –C**H$_2$**–CH$_2$–OH), 1.03 (*m*, 14.0**H**, SiC**H$_2$**CH$_2$CF$_3$), 0.93 (*t*, 2.0**H**, –C**H$_2$**–CH$_2$–CH$_2$–OH). ^{13}C {H} NMR (ppm, acetone-d_6): 4.7 (*m*, Si–**C**H$_2$–CH$_2$–CF$_3$), 27.5 (*m*, –CH$_2$–**C**H$_2$–CF$_3$, $J = 23$ Hz), 128.2 (*tetra*, –CH$_2$–CH$_2$–**C**F$_3$, $J = 274$ Hz); 9.5 (*m*, Si–**C**H$_2$–CH$_2$–CH$_2$Cl), 26.4 (*s*, –CH$_2$–**C**H$_2$–CH$_2$Cl), 47.0 (*s*, –CH$_2$–CH$_2$–**C**H$_2$Cl); ^{29}Si NMR (ppm, acetone-d_6): −69.4 (*s*, 3.0**Si**), −68.4 (*s*, 1.0**Si**), −67.0 (*s*, 3.1**Si**) and −66.1 (*s*, 1.0**Si**).

2.1.3. Synthesis of 3-trimethylsilyetherpropylhepta(3,3,3-trifluoropropyl) POSS

In order to confirm the formation of 3-hydroxypropylhepta (3,3,3-trifluoropropyl) POSS, the derivative of the aforementioned product was prepared and subjected to ^{1}H NMR analysis. 3-Hydroxypropylhepta (3,3,3-trifluoropropyl) POSS (1.0 g, 0.87 mmol), anhydrous THF (10 ml) and triethylamine (0.44 g, 4.35 mmol) were charged into a flask. Then the flask was immerged into an ice-water bath and chlorotrimethylsilane (0.47 g, 4.35 mmol) was added into the flask dropwise *via* a syringe. The mixture was reacted at 0 °C for 3 h and another 24 h at room temperature with vigorous stirring. After the insolvable solids were removed, the volatile components were removed *via* rotary evaporation to obtain solid products which were further dried in a vacuum oven at 40 °C for 24 h with a yield of 90%. ^{1}H NMR (ppm, acetone-d_6): 3.62 (*t*, 2.0**H**, –C**H$_2$**–OSi(CH$_3$)$_3$), 2.32 (*m*, 14.0**H**, SiCH$_2$C**H$_2$**CF$_3$), 1.93 (*m*, 2.0**H**, –C**H$_2$**–CH$_2$–O Si(CH$_3$)$_3$), 1.03 (*m*, 14.0**H**, SiC**H$_2$**CH$_2$CF$_3$), 0.93 (*t*, 2.0**H**, –C**H$_2$**–CH$_2$–CH$_2$–O Si(CH$_3$)$_3$), 0.09 (*s*, 9.0**H**, Si–CH$_2$CH$_2$CH$_2$–O–Si(C**H$_3$**)$_3$). It should be pointed out that in the NMR measurements no TMS was used as the internal reference.

2.1.4. Synthesis of POSS-capped PCL

The POSS-capped PCL was prepared by the ring-opening polymerization of ε-caprolactone which was initiated by 3-hydroxypropylhepta(3,3,3-trifluoropropyl) POSS and stannous (II) octanoate [Sn(Oct)$_2$] was used as a catalyst. Typically, 3-hydroxypropylhepta(3,3,3-trifluoropropyl) POSS (1.0 g, 0.86 mmol) and ε-caprolactone (4.7 g, 0.04 mol) were added to a pre-dried flask equipped with a magnetic stirrer. The flask was connected to a standard Schlenk line and the system was degassed *via* three pump-freeze-thaw cycles, and then the flask was put into an oil bath at 120 °C with vigorous stirring and Sn(Oct)$_2$ (1/1000 wt with respect to ε-CL) was added using a syringe. The pump-freeze-thaw process was carried out again and then the flask was immersed in a thermostated oil bath at 120 °C for 24 h. After completion of the polymerization, the crude products were dissolved in 10 ml THF and precipitated in 100 ml methanol. The procedures of dissolving and precipitation were repeated for 3 times to purify the products which were dried in vacuum oven at 35 °C for 24 h. ^{1}H NMR (ppm, CDCl$_3$): 0.92 (SiC**H$_2$**CH$_2$CF$_3$), 2.13 2.32 (SiCH$_2$C**H$_2$**CF$_3$), 0.84 (–C**H$_2$**–CH$_2$–CH$_2$–O–PCL), 1.84 (–C**H$_2$**–CH$_2$–O–PCL), 4.21 (–C**H$_2$**–O–PCL), 2.29 [–OCOC**H$_2$**(CH$_2$)$_4$–], 1.64 (–OCOCH$_2$C**H$_2$**CH$_2$C**H$_2$**CH$_2$O–), 1.37 (–OCOCH$_2$CH$_2$C**H$_2$**CH$_2$CH$_2$O–), 4.06 [–OCO(CH$_2$)$_4$C**H$_2$**–], 3.65 (–C**H$_2$**OH, terminal hydroxymethyl group). The molecular weight of the PCL was calculated in terms of the ratio of integration intensity of 4.21 ppm proton to 4.06 ppm protons in ^{1}H NMR spectrum to be $M_n = 5000$.

2.2. Preparation of nanostructured thermosets

The desired amount of DGEBA and POSS-capped PCL was mixed at 70 °C with continuous stirring for sufficiently long time until the homogeneous solutions were obtained. The curing agent, MOCA was then added into the mixture with vigorous stirring until the systems became homogeneous. The mixtures were poured into aluminum foil moulds. The samples were cured at 80 °C for 2 h and 150 °C for 3 h together with a post-cure at 180 °C for 2 h to attain the complete curing reaction. The thermosetting blends containing POSS-capped PCL up to 20 wt% were obtained.

2.3. Measurement and techniques

2.3.1. Fourier transform infrared spectroscopy (FTIR)

The FTIR measurements were conducted on a Perkin–Elmer Paragon 1000 Fourier transform spectrometer at room temperature (25 °C). The sample films were prepared by dissolving the polymers with THF (5 wt%) and the solutions were cast onto KBr windows. The residual solvent was removed in a vacuum oven at 60 °C for 2 h. The samples of thermosets were mixed with the powder of KBr and then pressed into the small flakes. All the specimens were sufficiently thin to be within a range where the Beer–Lambert law is obeyed. In all cases 64 scans at a resolution of 2 cm^{-1} were used to record the spectra.

2.3.2. Nuclear magnetic resonance spectroscopy (NMR)

The ^{1}H and ^{13}C NMR measurements were carried out on a Varian Mercury Plus 400 MHz NMR spectrometer. The samples were dissolved with deuterated acetone (acetone-d_6) or deuterated chloroform and the solutions were measured with tetramethylsilane (TMS) as the internal reference. The ^{29}Si NMR spectrum was obtained using a Brucker Avance III 400 400 MHz NMR spectrometer.

2.3.3. Atomic force microscopy (AFM)

The thermoset samples were trimmed using a microtome machine and the specimen sections (*ca.* 70 nm in thickness) were used for AFM observations. The AFM experiments were performed with a Nanoscope IIIa scanning probe microscope (Digital Instruments, Santa Barbara, CA, USA). Tapping mode was employed in air using a tip fabricated from silicon (125 mm in length with *ca.* 500 kHz resonant frequency). Typical scan speeds during recording were 0.3–1 line/s using scan heads with a maximum range of 1 μm × 1 μm.

2.3.4. Differential scanning calorimetry (DSC)

The calorimetric measurement was performed on a Perkin–Elmer Pyris-1 differential scanning calorimeter in a dry nitrogen atmosphere. The instrument was calibrated with standard Indium. All the samples (about 10 mg in weight) were heated from 0 to 200 °C and the DSC curves were recorded at a heating rate of 20 °C/min. The glass transition temperatures were taken as the midpoint of the capacity change.

2.3.5. Thermogravimetric analysis (TGA)

A Perkin–Elmer thermal gravimetric analyzer (TGA-7) was used to investigate the thermal stability of the hybrids. The samples (about 10 mg) were heated under nitrogen atmosphere from ambient temperature to 800 °C at the heating rate of 20 °C/min. The thermal degradation temperature was taken as the onset temperature at which 5 wt% of weight loss occurs.

2.3.6. Contact angle measurements

The flat free surfaces of the thermosets were used for the measurement of contact angle. The static contact angle measurements

with the probe liquids (*i.e.*, ultra-pure water and ethylene glycol) were carried out on a KH-01-2 contact angle measurement instrument (Beijing Kangsente Scientific Instruments Co., China) at room temperature. The samples were dried at 60 °C in a vacuum oven for 24 h prior to measurement.

2.3.7. X-ray photoelectron spectroscopy (XPS)

The XPS was measured with VG ESCALAB MK II at room temperature by using an Mg KR X-ray source ($h_\nu = 1253.6$ eV) at 14 kV and 20 mA. The sample analysis chamber of the XPS instrument was maintained at a pressure of 1×10^{-7} Pa. To determine the composition on the top layer of the film, the tilting angle is 5°. The binding energies were calibrated by using the containment carbon (C1s = 284.6 eV). A linear background method removed the XPS background and the peak analyses carried out by using the curve-fitting software.

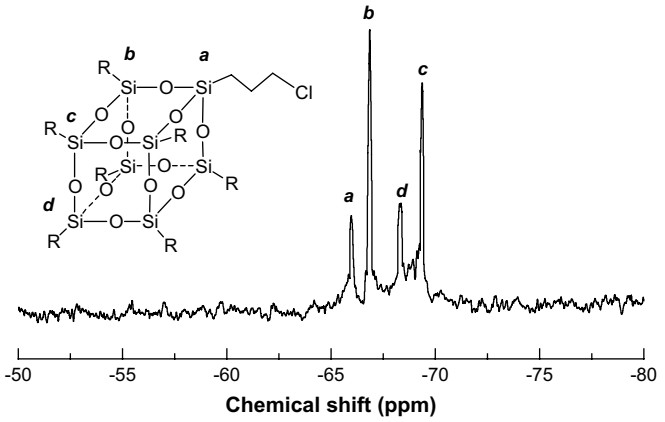

Fig. 1. ^{29}Si NMR spectrum of 3-chloropropylhepta(3,3,3-trifluoropropyl) POSS.

3. Results and discussion

3.1. Synthesis of POSS-capped PCL

The route of synthesis for hepta(3,3,3-trifluoropropyl) POSS-capped PCL is shown in Scheme 2. In the first step, hepta(3,3,3-trifluoropropyl)tricycloheptasiloxane trisodium silanolate [$Na_3O_{12}Si_7(C_3H_4F_3)_7$] was prepared by following the method reported by Fukuda et al. [25]. The corner-capping reaction between $Na_3O_{12}Si_7(CH_2CH_2CF_3)_7$ and 3-chloropropyltrichlorosiloxane was carried out to afford 3-chloropropylhepta(3,3,3-trifluoropropyl) POSS. Shown in Fig. 1 is the ^{29}Si NMR spectrum of 3-chloropropylhepta(3,3,3-trifluoropropyl) POSS. The resonance at −70.1 ppm is assignable to the corner silicon atom connected with 3-chloropropyl group; the resonance at −69.2, −66.7 and −65.9 ppm is ascribed to the other silicon nucleus of silsesquioxane with the distance from far to close far from the corner silicon atom. In terms of the ratio of integration intensity of the resonance [25], it is judged that the octameric silsesquioxane was formed. The ^{1}H NMR spectroscopy further shows that the molar ratio of 3-chloropropyl to 3,3,3-trifluoropropyl groups is quite close to 1:7 according to the ratio of integration intensity of 3-chloropropyl to 3,3,3-trifluoropropyl protons in the ^{1}H NMR spectrum of the product. The 3-chloropropyl group of the POSS macromer was then converted into 3-hydroxypropyl groups *via* the substitution reaction of chlorine atom with hydroxyl group. To promote the reaction to completion, freshly made Ag_2O was added to the system. The ^{1}H NMR spectroscopy was employed to quantify the above substitution reaction and the ^{1}H NMR spectra of 3-chloropropylhepta(3,3,3-trifluoropropyl) POSS and 3-hydroxypropylhepta(3,3,3-trifluoropropyl) POSS are presented in Fig. 2. Unfortunately, the chemical shifts of methylene protons connected to the chlorine atom and hydroxyl groups for the two POSS compounds are too close to be used for the evaluation of the substitution reaction. Therefore, we prepared the derivative of 3-hydroxypropylhepta(3,3,3-trifluoropropyl) POSS *via* its silylation with trimethylchlorosilane [$ClSi(CH_3)_3$]. The derivative was subjected to ^{1}H NMR measurement and the ^{1}H NMR spectrum was also shown in Fig. 2. The resonance at 0.09 ppm is assignable to the proton of methyl groups of the derivative. According to the ratio of

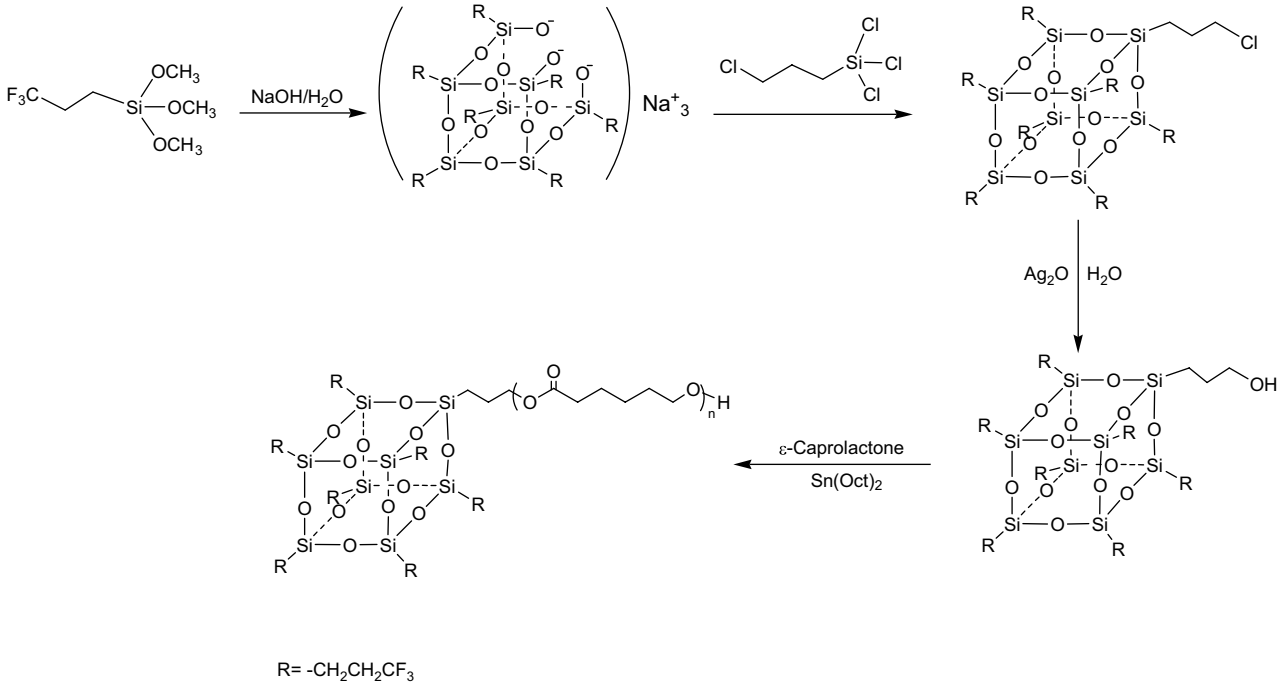

Scheme 2. Synthesis of POSS-capped PCL.

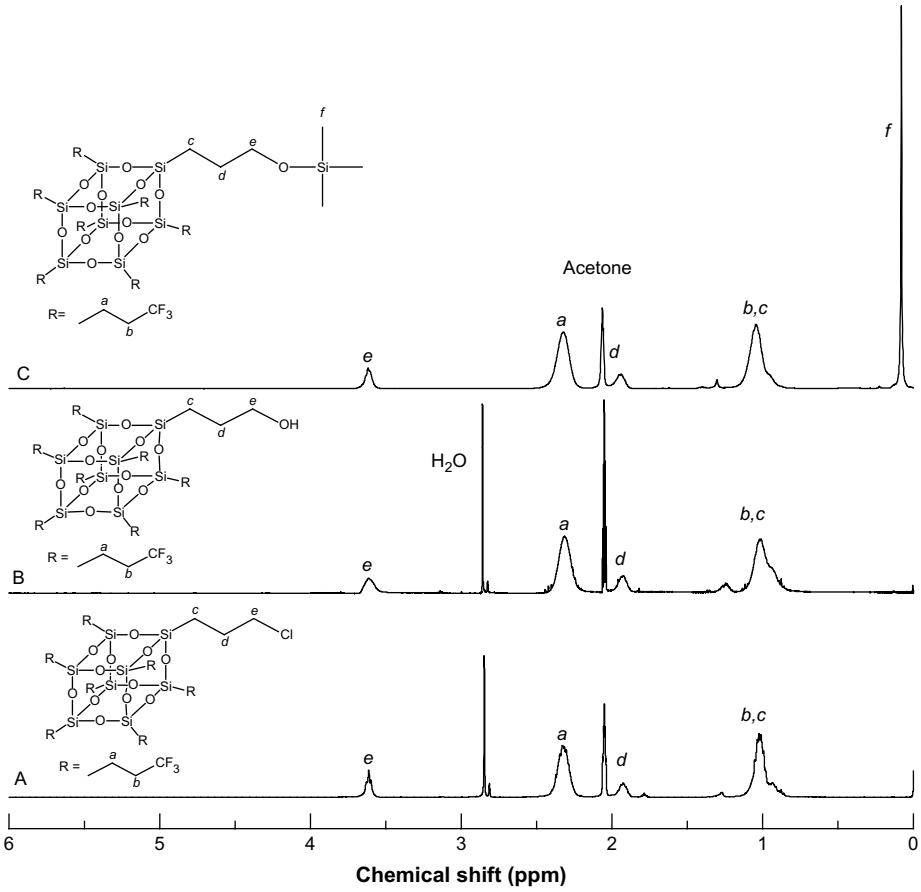

Fig. 2. ^{1}H NMR spectra of (A) 3-chloropropylhepta(3,3,3-trifluoropropyl) POSS, (B) 3-hydroxypropylhepta(3,3,3-trifluoropropyl) POSS and (C) 3-trimethylsilyether propylhepta(3,3,3-trifluoropropyl) POSS.

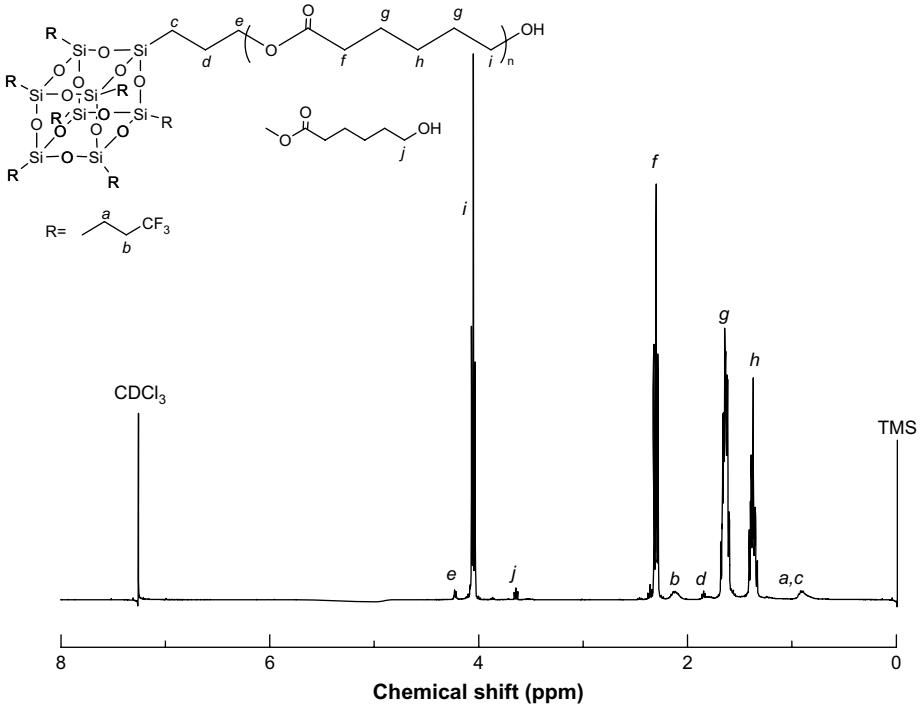

Fig. 3. ^{1}H NMR spectrum of POSS-capped PCL.

integration intensity of methyl to those of methylene protons, it is judged that the 3-hydroxypropylhepta(3,3,3-trifluoropropyl) POSS was successfully synthesized. It should be pointed out that the occurrence of the substitution reaction did not affect the octameric silsesquioxane structure, which is evidenced by ^{29}Si NMR spectroscopy. The similar result has been reported for the conversion of 3-chloropropylheptaphenyl POSS into 3-hydroxypropylheptaphenyl POSS [33].

3-Hydroxypropylhepta(3,3,3-trifluoropropyl) POSS was further used as the initiator for the ring-opening polymerization reaction of ε-caprolactone (CL) to afford the hepta(3,3,3-trifluoropropyl) POSS-capped PCL. The polymerization was carried out at 120 °C for 24 h with stannous (II) octanoate [Sn(Oct)$_2$] as the catalyst. By controlling the molar ratio of 3-hydroxypropylhepta(3,3,3-trifluoropropyl) POSS to CL, the POSS-capped PCL with desired molecular weights was obtained. The length of PCL chain can be estimated in terms of the ratio of integration intensity of terminal methylene protons of PCL chain to those of other methylene protons in its ^{1}H NMR spectrum (see Fig. 3). In this work, the length of the PCL chain was calculated to be about $M_n = 5000$, which is quite close to that estimated according to the conversion of CL monomer. This result indicates that the POSS-capped PCL was successfully obtained. The POSS-capped PCL was subjected to differential scanning calorimetry (DSC) and the thermograph is presented in Fig. 4. It is seen that a single endothermic transition was displayed at 56 °C, which is assignable to the melting transition of PCL chains of the organic–inorganic amphiphile. The DSC shows that the POSS-capped PCL is a semicrystalline organic–inorganic amphiphile.

3.2. Morphology of thermosets

The POSS-capped PCL amphiphile was incorporated into epoxy to prepare the nanostructured hybrids. Before curing, all the ternary mixtures composed of DGEBA, POSS-capped PCL and MOCA were homogeneous and transparent. After cured at the elevated temperatures, the epoxy thermosets with the POSS-capped PCL contents up to 20 wt% were obtained. All the cured products investigated are homogeneous and clear, suggesting that no macroscopic phase separation occurred at the scale exceeding the wavelength of visible lights with the occurrence of curing reaction. The morphologies of the thermosets were examined by means of atomic force microscopy (AFM). Shown in Fig. 5 are the AFM images of the epoxy thermosets containing POSS-capped PCL. The left and right images are the topography and phase contrast images, respectively. In terms of the volume fraction of POSS and the

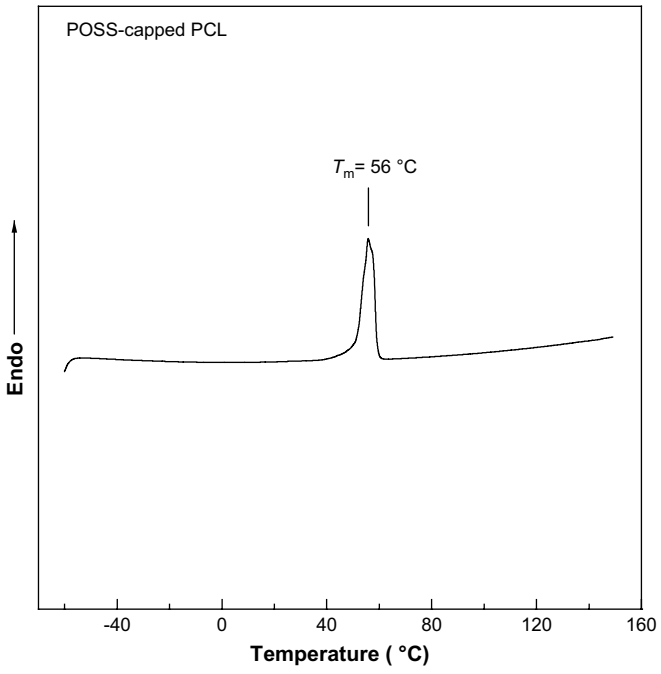

Fig. 4. DSC curve of POSS-capped PCL.

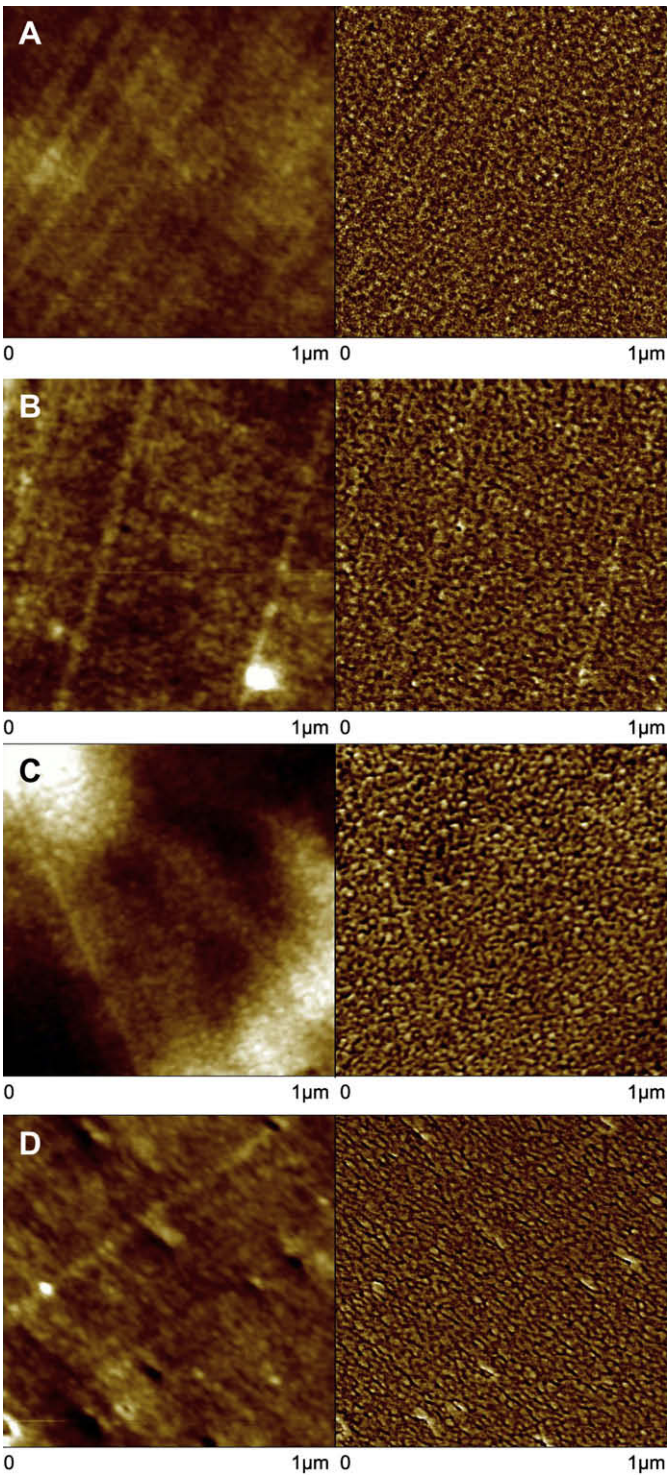

Fig. 5. AFM micrographs of epoxy thermosets containing: (A) 5, (B) 10, (C) 15 and (D) 20 wt% POSS-capped PCL. Left: topography; right: phase contrast.

difference in viscoelastic properties between epoxy matrix and POSS phases, the light continuous regions are assignable to the crosslinked epoxy matrix, which could be miscible with the PCL chains of the organic–inorganic amphiphile whilst the dark regions are attributed to POSS domains. It is seen that all the thermosets exhibited microphase-separated morphologies. For the thermoset containing 10 wt% of POSS-capped PCL the nanoscaled POSS spherical particles with the size of 10–20 nm were homogenously dispersed in the continuous epoxy matrix. With increasing the content of POSS-capped PCL, some interconnected POSS microdomains began to appear (Fig. 5B) and the quantity of the POSS microdomains was increased whereas the size of the spherical particle remains almost invariant (Fig. 5B–D).

3.3. Interpretation of self-assembly behavior

The POSS-capped PCL is a typical organic–inorganic amphiphile. Depending on the miscibility of sub-component of the organic–inorganic amphiphile (*i.e.*, POSS moiety and PCL chains) with epoxy after and before curing reaction, the formation of nanostructures in the composite system could follow the so-called reaction-induced microphase separation [34–43] or self-assembly mechanism [44–57]. The mechanistic difference between the two approaches rests with the miscibility of the sub-components of the POSS-capped PCL with epoxy after and before curing reaction. For the mechanism of reaction-induced microphase separation (RIMS), it is required that all the sub-components of the POSS-capped PCL are miscible with the epoxy before curing reaction and the microphase separation only occur with the proceeding of the curing reaction. For the mechanism of self-assembly, it is required that one sub-component of the organic–inorganic amphiphile must be immiscible whereas the other sub-component remains miscible with epoxy before curing reaction. In this case, the organic–inorganic amphiphile was self-organized into the nanostructures before curing reaction, which can be fixed *via* the subsequent curing reaction. In the present system, it has been known that PCL chains are miscible with epoxy after and before curing reaction [58,59]. It is necessary to investigate the miscibility of the POSS with epoxy resin after and before curing reaction. To this end, 3-chloropropylhepta(3,3,3-trifluoropropyl)POSS [or 3-hydroxyhepta(3,3,3-trifluoropropyl)POSS] was selected as the model compound of the POSS. It was seen that before and after curing reaction, the mixtures composed of 3-chloropropylhepta(3,3,3-trifluoropropyl)POSS [or 3-hydroxyhepta(3,3,3-trifluoropropyl)POSS] are cloudy and be macroscopically phase separated at room and elevated temperatures (*e.g.*, 150 °C). This observation indicates that the POSS portion is immiscible with epoxy before and after curing reaction. The immiscibility of POSS with epoxy resin suggests that the formation of the nanostructure in the present system followed the mechanism of self-assembly. Therefore, it is proposed that the nanostructures in the thermosets actually resulted from the preformed templates before curing reaction. The curing reaction locked in (or fixed) the preformed self-organized structures. The formation of nanostructures is depicted in Scheme 3.

It should be pointed out that the PCL chains remain miscible with epoxy in the organic–inorganic composite systems after and before curing reaction. Before curing reaction, the miscibility of PCL with the precursors of epoxy (*i.e.*, DGEBA and MOCA) is ascribed to the non-negligible contribution of mixing entropy (ΔS_m) to free energy of mixing (ΔG_m). After curing reaction, the PCL chains were still miscible with the epoxy thermosets. This judgment can be evidenced by means of glass transition behavior of the nanostructured epoxy thermosets. The above nanostructured epoxy thermosets were subjected to thermal analyses and the DSC thermograms are shown in Fig. 6. For the POSS-capped PCL, a single endothermic transition was displayed at 56 °C (see Fig. 4), which is assignable to the melting transition of PCL chains of the organic–inorganic amphiphile. Nonetheless, it is noted that all the thermosets containing the POSS-capped PCL did not exhibit the melting transition of PCL subchains, suggesting that the PCL subchains were not crystallizable in the nanostructured thermosets. It is proposed that the PCL subchains are miscible with the epoxy thermosets, *i.e.*, they interpenetrated with the crosslinked epoxy networks. The miscibility was further demonstrated by the depression in glass transition temperatures (T_gs) for the epoxy matrix (see Fig. 6). Each thermoset containing POSS-capped PCL displayed single T_g, which are intermediate between the T_gs of the pure components. It is seen that the T_gs decreased with increasing the concentration of POSS-capped PCL. The decreased T_gs resulted from the plasticization effect of miscible PCL on epoxy matrix.

The miscibility of PCL chains with the epoxy matrix can be attributed to the intermolecular hydrogen-bonding interactions between the carbonyl groups of PCL and the hydroxyl groups in the hydroxyether structural units of the aromatic amine-cured diglycidyl ether of bisphenol A. The intermolecular hydrogen-bonding interactions are readily investigated by means of Fourier transform infrared spectroscopy (FTIR). Shown in Fig. 7 are the FTIR spectra of the POSS-capped PCL and the organic–inorganic nanocomposites containing variable amount of POSS-capped PCL in the range of 1680–1780 cm^{-1}. The absorption bands in this region are ascribed to the stretching vibration of carbonyl groups (>C=O) of PCL chains. At the room temperature, the carbonyl band of the pure POSS-capped PCL consists of two components sensitive to the conformation of PCL chains (see Fig. 7E). The one component centered at 1735 cm^{-1} is characteristic of amorphous chains of PCL whereas the sharp band at 1725 cm^{-1} is ascribed to the carbonyls in

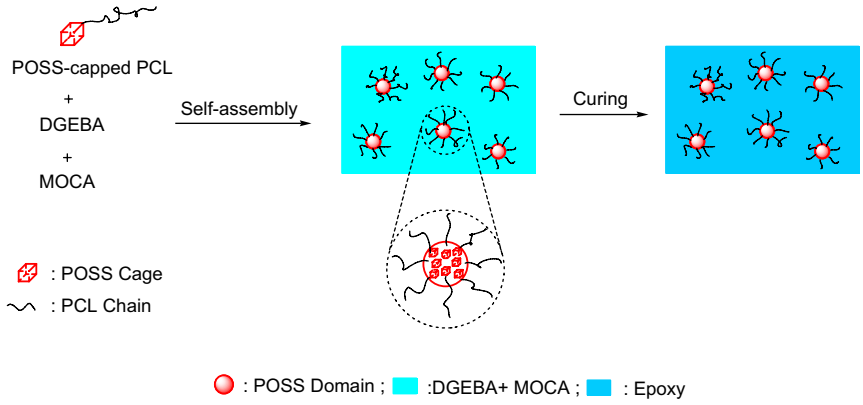

Scheme 3. Formation of nanostructures in epoxy thermosets containing POSS-capped PCL.

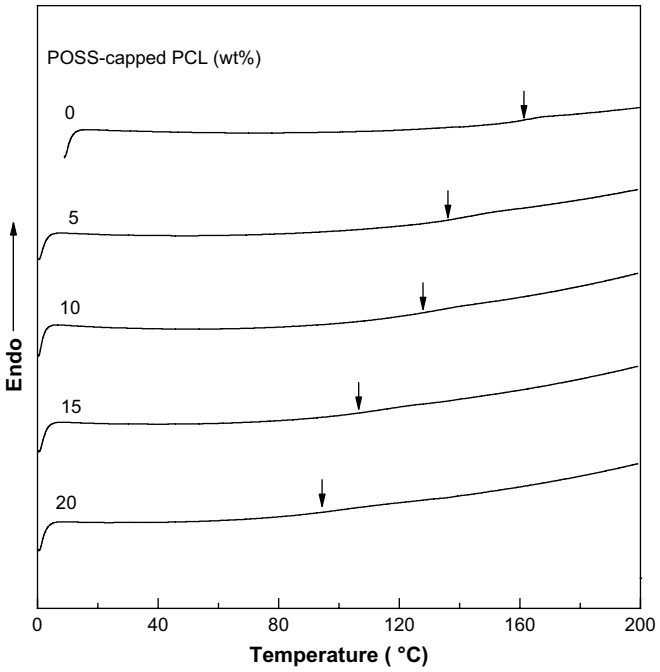

Fig. 6. DSC curves of organic–inorganic hybrids thermosets containing POSS-capped PCL.

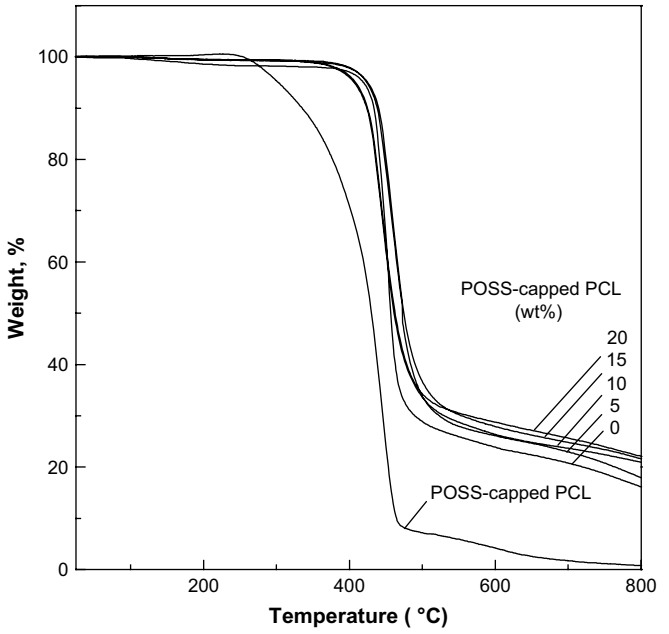

Fig. 8. TGA curves of POSS-capped PCL and POSS-capped PCL-containing epoxy thermosets.

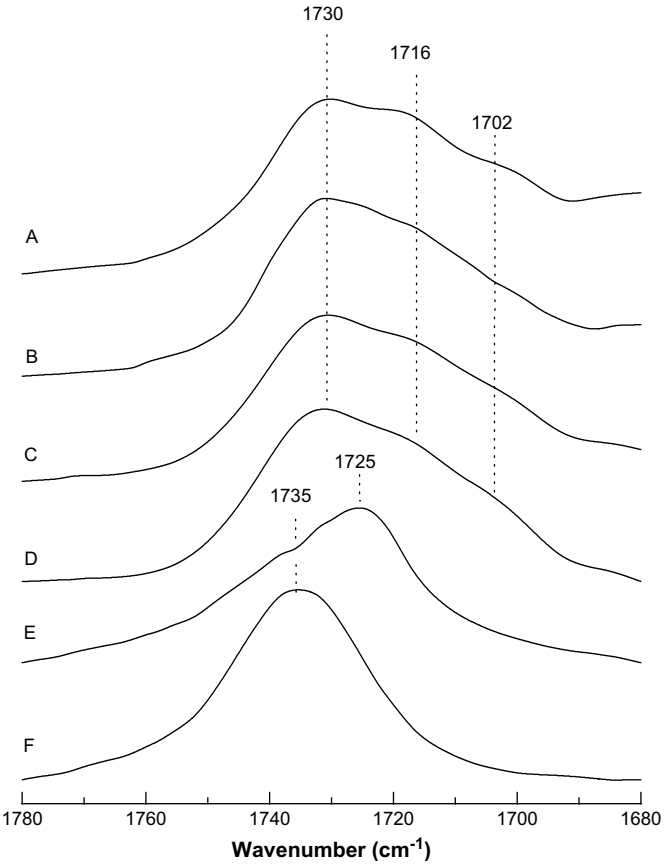

Fig. 7. FTIR spectra of thermosets containing (A) 20; (B)15; (C)10; (D) 5 wt% POSS-capped PCL and (E) POSS-capped PCL at 25 °C; (F) POSS-capped PCL at 80 °C.

the crystalline region of PCL. Upon heating the organic–inorganic amphiphile up to 80 °C, the band at 1725 cm^{-1} disappeared owing to the fusion of PCL crystals (see Fig. 7F). For the POSS-capped PCL-containing epoxy thermosets, the bands of PCL crystals at 1725 cm^{-1} were absent, implying that the PCL chains exist in the materials in the amorphous state. This observation is in good agreement with DSC. It is noted that there, nonetheless, appeared new shoulders at the lower frequencies of 1702 and 1716 cm^{-1} in the FTIR spectra (see Fig. 7A–D). The shoulder bands are assigned to the stretching vibration of hydrogen-bonded carbonyls [60,61], *i.e.*, there is the formation of the intermolecular hydrogen-bonding interactions between the secondary hydroxyl groups of epoxy matrix and the carbonyl groups of PCL. In addition, the bands at 1735 cm^{-1} were found to shift to the lower frequency (1730 cm^{-1}) with increasing the concentration of the POSS-capped PCL. The FTIR results indicate that there existed the intermolecular hydrogen-bonding interactions between the PCL chains of POSS-capped PCL and the epoxy networks. In other words, the PCL chains were intimately mixed with the epoxy matrix in the organic–inorganic hybrid nanocomposites.

3.4. Thermal and surface properties of thermosets

Thermogravimetric analysis (TGA) was applied to evaluate the thermal stability of the POSS-containing nanocomposites. Shown in Fig. 8 are the TGA curves of the control epoxy and the nanocomposites, recorded in nitrogen atmosphere at 20 °C/min. Within the experimental temperature range, all the samples displayed

Table 1
Values of static contact angle and surface energy.

POSS-capped PCL (wt%)	Contact angle		Surface energy		
	Water	Ethylene glycol	γ_S^d	γ_S^p	γ_S
0	74.3	60.7	9.1	20.3	29.4
5	93.8	71.1	17.2	4.8	22.0
10	96.5	77.2	14.7	4.1	18.8
15	100.4	82.1	13.0	3.3	16.3
20	108.2	88.0	14.3	1.1	15.4

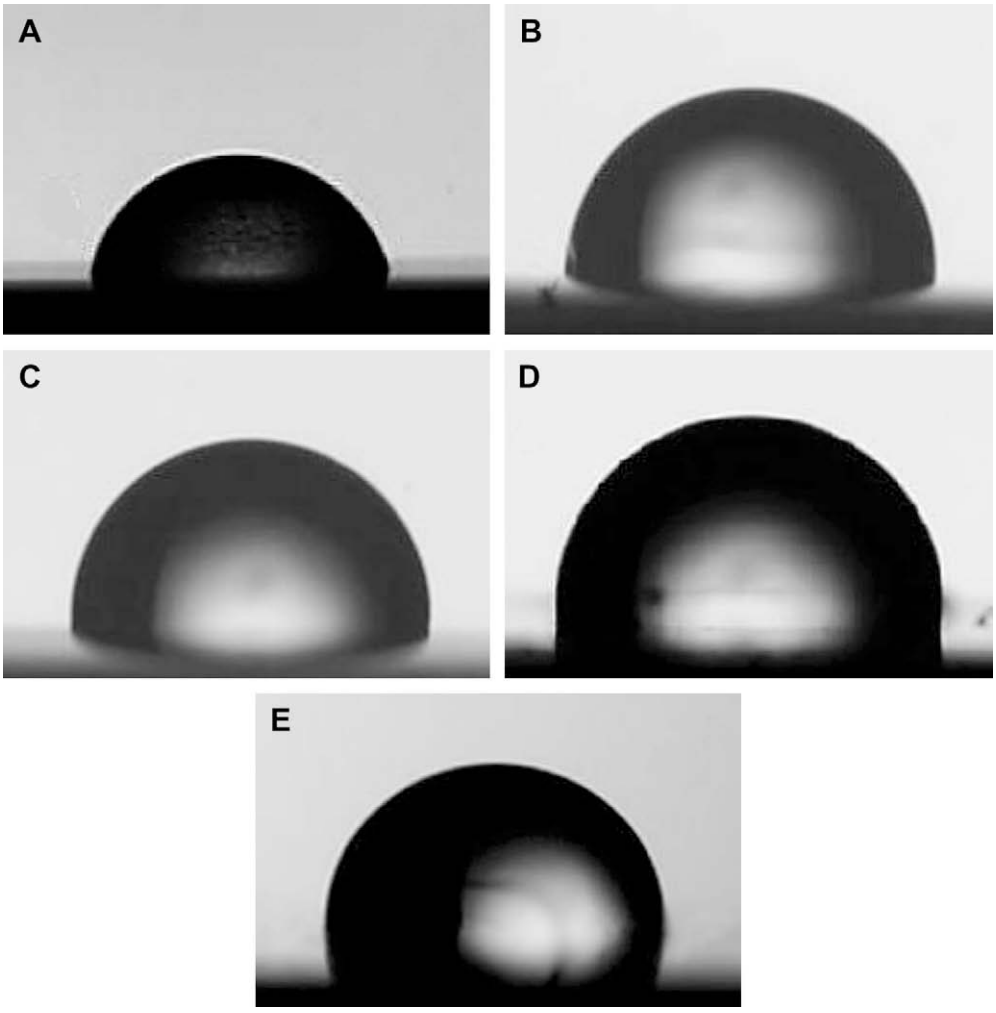

Fig. 9. Water contact angle images on the surface of nanostructured epoxy thermosets containing POSS-capped PCL.

similar degradation profiles, suggesting that the existence of POSS-capped PCL did not significantly alter the degradation mechanism of the matrix polymers. Compared to the control epoxy, the initial decomposition temperature of the hybrid nanocomposites slightly decreased with increasing the concentration of POSS-capped PCL. The decreased initial decomposition temperature could result from the inclusion of PCL portion, which possesses the lower thermal stability than the control epoxy. However, it is noted that the nanocomposites displayed increased the yield of degradation residues due to the inclusion of organic–inorganic amphiphile. The summation of char and ceramic yields increased with increasing the content of POSS-capped PCL.

The POSS moiety of the organic–inorganic amphiphile used in this work contains organosilicon and organofluorine moieties and is of low free energy [25–32]. It is expected that the enrichment of the POSS portion at the surface of the thermosetting materials will occur upon incorporating the POSS-capped PCL into organic polymer. This effect can be reflected with the enhancement of the surface hydrophobicity of the hybrid thermosets [25–32], which was readily examined by means of contact angle measurements and surface element analysis. The static surface contact angles were measured with water and ethylene glycol as probe liquids and the results are summarized in Table 1. The contact angle of the control epoxy resin was estimated with water to be 74.3°. Upon adding POSS-capped PCL to the system the water contact angles are dramatically enhanced. The contact angles increased with increasing the content

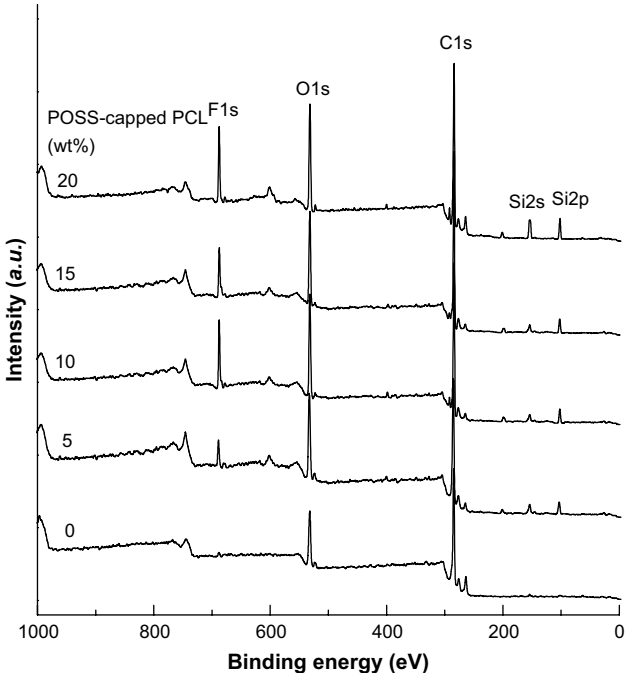

Fig. 10. XPS spectra of epoxy thermosets containing POSS-capped PCL.

Table 2
Elemental compositions of surfaces for epoxy thermosets containing POSS-capped PCL determined by means of XPS.

POSS-capped PCL (wt%)	Calculated (mol%)						Experimental (mol%)					
	C	O	Si	F	N	Cl	C	O	Si	F	N	Cl
5	81.7	12.4	0.07	0.2	2.8	2.8	73.8	18.3	1.4	3.6	1.6	1.3
10	81.4	12.8	0.13	0.4	2.6	2.6	59.7	23.8	4.9	9.3	1.0	1.3
15	81.2	13.3	0.2	0.6	2.3	2.3	51.2	27.0	7.2	11.9	1.7	1.0
20	80.8	13.9	0.28	0.8	2.1	2.1	54.3	23.4	8.4	12.0	0.8	1.1

of POSS-capped PCL (see Fig. 9). When the content of POSS-capped PCL is 20 wt%, the water contact angle of the nanocomposites is 108.2°, which is higher than that of the control epoxy by 30°. This observation indicates that the hydrophobicity of the materials is significantly enhanced [62,63]. The surface free energies of the hybrid nanocomposites containing various percentages of POSS-capped PCL were calculated according to the geometric mean model [64–66]:

$$\cos\ \theta = \frac{2}{\gamma_L}\left[\left(\gamma_L^d\gamma_s^d\right)^{\frac{1}{2}}+\left(\gamma_L^p\gamma_s^p\right)^{\frac{1}{2}}\right]-1 \quad (1)$$

$$\gamma_s = \gamma_s^d+\gamma_s^p \quad (2)$$

where θ is the contact angle and γ_L is the liquid surface tension; γ_s^d and γ_s^p are the dispersive and polar components of γ_L, respectively. From Table 1, it is seen that with the increase of the POSS content, the total surface free energies of the composites were reduced from 29.37 mN/m to 15.35 mN/m. It is noted that the polar component is very sensitive to the concentration of POSS, suggesting that the inclusion of POSS moiety significantly changed the distribution of the polar groups on the surface energy of materials, *i.e.*, the POSS moiety on the surface acts as a screening agent to the polar groups of epoxy resin. The enrichment of POSS moiety of the organic–inorganic amphiphile on the surface of the nanostructured thermosets can be confirmed by means of X-ray photoelectron spectroscopy (XPS). Shown in Fig. 10 are the XPS spectra of the control epoxy and its nanocomposites containing POSS-capped PCL. The C1s peak was observed at about 286.8 eV, which was responsible for the contribution of several kinds of carbon atoms from the epoxy thermoset and POSS-capped PCL. The O1s peak was at approximately 535 eV. The signals of Cl and N are assignable to the MOCA moiety. The Si atoms from silsesquioxane moiety of POSS-capped PCL contributed the Si 2s, Si 2p signals at 156 and 105 eV, respectively. The F1s peak was detected at 688 eV, which results from the 3,3,3-trifluoroprophyl groups of POSS. The relative concentrations of C, O, N, Cl, Si and F elements on the surfaces of the organic–inorganic hybrid composites, calculated from the corresponding photoelectron peak areas are listed in Table 2. It is seen that the carbon and oxygen were dominant on the detected surfaces of all the nanostructured thermosets and a small amount of nitrogen and chlorine from MOCA moiety was also detected. It is noticed that the concentrations of elements Si and F on the surface of the nanostructured thermosets are significantly higher than the theoretical values calculated in terms of feed ratios. The surface contents of Si and F elements increased with increasing POSS-capped PCL in the nanostructured thermosets. For instance, the surface contents of Si and F elements are 8.4 and 12.0 mol%, respectively, for the nanocomposites containing 20 wt% POSS-capped PCL, which are much higher than those of the theoretical value for this nanocomposite. This observation suggests that there exists the enrichment of Si(or F)-containing moiety on the surfaces of the nanostructured thermosets. This result is important to understand the improvement in surface hydrophobicity for the nanocomposites. It is worth noticing that the enrichment of Si and F elements on the surfaces of the nanocomposites does not monotonously increase with increasing the concentration of POSS-capped PCL in the thermosets, which could be related to the nanostructures of the thermosets.

4. Conclusions

Hepta(3,3,3-trifluoropropyl) polyhedral oligomeric silsesquioxane-capped poly(ε-caprolactone) (POSS-capped PCL) was synthesized *via* ring-opening reaction of ε-caprolactone, which was initiated by 3-hydroxypropylhepta(3,3,3-trifluoropropyl) polyhedral oligomeric silsesquioxane with $Sn(Oct)_2$ as the catalyst. The organic–inorganic amphiphile was incorporated into epoxy to prepare the nanostructured organic–inorganic hybrids. The nanostructures of the hybrids were investigated by means of atomic force microscopy (AFM). The formation of nanostructures was addressed on the basis of miscibility and phase behavior of the subcomponents of the organic–inorganic amphiphile with epoxy after and before curing reaction. It is proposed that the formation of the nanostructures followed the mechanism of self-assembly. The static contact angle measurements indicate that the organic–inorganic nanocomposites displayed a significant enhancement in surface hydrophobicity as well as reduction in surface free energy. The improvement in surface properties was ascribed to the enrichment of POSS moiety on the surface of the nanostructured thermosets.

Acknowledgments

The financial supports from Natural Science Foundation of China (No. 20474038 and 50873059) and National Basic Research Program of China (No. 2009CB930400) are acknowledged. The authors thank Shanghai Leading Academic Discipline Project (Project Number: B202) for the partial support.

References

[1] Whitesides GM, Mathias JP, Seto CT. Science 1991;254:1312–9.
[2] Brinker CJ, Scherer GC. Sol–gel science: the physics and chemistry of sol–gel processing. Academic Press; 1990.
[3] Giannelis EP, Krishnamoorti R, Manias E. Adv Polym Sci 1999;138:107–47.
[4] Schwab JJ, Lichtenhan JD. Appl Organomet Chem 1998;12:707–13.
[5] Li G, Wang L, Ni H, Pittman CU. J Inorg Organomet Polym 2001;11:123–54.
[6] Abe Y, Gunji T. Prog Polym Sci 2004;29:149–82.
[7] Lee A, Lichtenhan JD. Macromolecules 1998;31:4970–4.
[8] Choi J, Harcup J, Yee AF, Zhu Q, Laine RM. J Am Chem Soc 2001;123:11420–30.
[9] Choi J, Kim SG, Laine RM. Macromolecules 2004;37:99–109.
[10] Laine RM, Choi J, Lee I. Adv Mater 2001;13:800–3.
[11] Choi J, Yee AF, Laine RM. Macromolecules 2003;36:5666–82.
[12] Choi J, Tamaki R, Kim SG, Laine RM. Chem Mater 2003;15:3365–75.
[13] Choi J, Yee AF, Laine RM. Macromolecules 2004;37:3267–76.
[14] Abad MJ, Barral L, Fasce DP, Williams RJJ. Macromolecules 2003;36:3128–35.
[15] Zucchi IA, Galante MJ, William RJJ, Franchini E, Galy J, Gerard J-F. Macromolecules 2007;40:1274–82.
[16] Liu H, Zheng S, Nie K. Macromolecules 2005;38:5088–97.
[17] Matejka L, Strachota A, Plestil J, Whelan P, Steinhart M, Slaof M. Macromolecules 2004;37:9449–56.
[18] Strachota A, Kroutilova I, Kovarova J, Matejka L. Macromolecules 2004;37:9457–64.
[19] Li GZ, Wang L, Toghiani H, Daulton TL, Koyama K, Pittman CU. Macromolecules 2001;34:8686–93.

[20] Lichtenhan JD, Feher FJ, Schwab JJ, Zheng S. Reactive grafting and compatibilization of polyhedral oligomeric silsesquioxanes. Hybrid Plastics, LLP; 2005. US Patent 6,933,345.
[21] Ni Y, Zheng S, Nie K. Polymer 2004;45:5557–68.
[22] Huang C-F, Kuo S-W, Lin F-J, Huang W-J, Wang C-F, Chen W-Y, et al. Macromolecules 2006;39:300–8.
[23] Ni Y, Zheng S. Macromolecules 2007;40:7009–18.
[24] Zeng K, Zheng S. J Phys Chem B 2007;111:13919–28.
[25] Koh K, Sugiyama S, Fukuda T. Macromolecules 2005;38:1264–70.
[26] Feast WJ, Munro HS, Richarsa RW, editors. Polymer surface and interface, II. Chichester: John Wiley & Sons; 1993.
[27] Affrossman S, Bertrand R, Hartshorne M, Kiff T, Leonard D, Pethrick RW. Macromolecules 1996;29:5432–7.
[28] Youngblood JP, McCarthy TJ. Macromolecules 1999;32:6800–6.
[29] Li XF, Chiellini E, Galli G, Ober CK, Hexemer A, Kramer EJ, et al. Macromolecules 2002;35:8078–87.
[30] Hirao A, Koide G, Sugiyama K. Macromolecules 2002;35:7642–51.
[31] O'Rourke-Muisener PAV, Jalbert CA, Yuan CG, Baezold J, Mason R, Wong D, et al. Macromolecules 2003;36:2956–66.
[32] Koberstein JT. J Polym Sci Part B Polym Phys 2004;42:2942–56.
[33] Ni Y, Zheng S. J Polym Sci Part A Polym Chem 2007;45:1247–59.
[34] Larrañaga M, Gabilondo N, Kortaberria G, Serrano E, Remiro P, Riccardi CC, et al. Polymer 2005;46:7082–93.
[35] Meng F, Zheng S, Zhang W, Li H, Liang Q. Macromolecules 2006;39:711–9.
[36] Serrano E, Tercjak A, Kortaberria G, Pomposo JA, Mecerreyes D, Zafeiropoulos NE, et al. Macromolecules 2006;39:2254–61.
[37] Meng F, Zheng S, Li H, Liang Q, Liu T. Macromolecules 2006;39:5072–80.
[38] Meng F, Zheng S, Liu T. Polymer 2006;47:7590–600.
[39] Sinturel C, Vayer M, Erre R, Amenitsch H. Macromolecules 2007;40:2532–8.
[40] Xu Z, Zheng S. Macromolecules 2007;40:2548–58.
[41] Meng F, Xu Z, Zheng S. Macromolecules 2008;41:1411–20.
[42] Ruiz-Pérez L, Royston GJ, Fairclough JA, Ryan AJ. Polymer 2008;49:4475–88.
[43] Fan W, Zheng S. Polymer 2008;49:3157–67.
[44] Hillmyer MA, Lipic PM, Hajduk DA, Almdal K, Bates FS. J Am Chem Soc 1997;119:2749–50.
[45] Lipic PM, Bates FS, Hillmyer MA. J Am Chem Soc 1998;120:8963–70.
[46] Mijovic J, Shen M, Sy JW, Mondragon I. Macromolecules 2000;33:5235–44.
[47] Grubbs RB, Dean JM, Broz ME, Bates FS. Macromolecules 2000;33:9522–34.
[48] Kosonen H, Ruokolainen J, Nyholm P, Ikkala O. Macromolecules 2001;34:3046–9.
[49] Ritzenthaler S, Court F, Girard-Reydet E, Leibler L, Pascault JP. Macromolecules 2002;35:6245–54.
[50] Ritzenthaler S, Court F, Girard-Reydet E, Leibler L, Pascault JP. Macromolecules 2003;36:118–26.
[51] Guo Q, Thomann R, Gronski W. Macromolecules 2003;36:3635–45.
[52] Dean JM, Verghese NE, Pham HQ, Bates FS. Macromolecules 2003;36:9267–70.
[53] Rebizant V, Abetz V, Tournihac T, Court F, Leibler L. Macromolecules 2003;36:9889–96.
[54] Rebizant V, Venet AS, Tournillhac F, Girard-Reydet E, Navarro C, Pascault JP, et al. Macromolecules 2004;37:8017–27.
[55] Gong W, Zeng K, Wang L, Zheng S. Polymer 2008;49:3318–26.
[56] Xu Z, Zheng S. Polymer 2007;48:6134–44.
[57] Guo Q, Liu J, Chen L, Wang K. Polymer 2008;49:1737–42.
[58] Yin M, Zheng S. Macromol Chem Phys 2005;206:929–37.
[59] Ni Y, Zheng S. Polymer 2005;46:5828–39.
[60] Coleman MM, Painter PC. Prog Polym Sci 1995;20:1–59.
[61] Coleman MM, Graf JF, Painter PC. Specific interactions and the miscibility of polymer blends. Lancaster, PA: Technomic Publishing; 1991.
[62] Mabry JM, Vij A, Iacono ST, Viers BD. Angew Chem Int Ed 2008;47:4137–40.
[63] Iacono ST, Vij A, Grabow W, Smith DW, Mabry JM. Chem Commun 2007;47:4992–4.
[64] Kaelble DH, Uy KC. J Adhes 1970;2:50–60.
[65] Kaelble DH. Physical chemistry of adhesion. New York: Wiley-Interscience; 1971.
[66] Adamson AW. Physical chemistry of surfaces. 5th ed. New York: Wiley-Interscience; 1990.